IEEE Access
Multidisciplinary | Rapid Review | Open Access Journal

Received June 13, 2019, accepted July 16, 2019, date of publication July 25, 2019, date of current version August 12, 2019.

Digital Object Identifier 10.1109/ACCESS.2019.2930994

Development of Underwater Drilling Robot Based on Earthworm Locomotion

KEITA ISAKA[1], KAZUKI TSUMURA[1], TOMOKI WATANABE[1], WATARU TOYAMA[2], MAKOTO SUGESAWA[3], YASUYUKI YAMADA[4,5], (Member, IEEE), HIROSHI YOSHIDA[3], AND TARO NAKAMURA[2], (Member, IEEE)

[1]Graduate School of Science and Engineering, Chuo University, Bunkyo-Ku 112-8551, Japan
[2]Faculty of Science and Engineering, Chuo University, Bunkyo-Ku 112-8551, Japan
[3]Marine Technology and Engineering Center, Japan Agency for Marine-Earth Science and Technology, Yokosuka 237-0061, Japan
[4]School of System Design and Technology, Tokyo Denki University, Chiyoda-Ku 120-8551, Japan
[5]Research and Development Initiative, Chuo University, Bunkyo-Ku 112-8551, Japan

Corresponding author: Keita Isaka (k_isaka@bio.mech.chuo-u.ac.jp)

ABSTRACT In this paper, a drilling robot based on earthworm locomotion was developed for seafloor exploration. Seabed mineral resources are found on the bottom of the ocean. The drilling robot developed herein can excavate and obtain samples of seafloor soil. This paper was inspired by the results of the previous study, in which a drilling robot based on earthworm locomotion developed for land successfully demonstrated the ability to create curved boreholes of 1670-mm turning radius and 613-mm depth. By principle, earthworm locomotion is propelled without rubbing the side of the robot against the wall of the borehole. That is, the movement is not affected by earth pressure, and thus it is facilitated deep into the soil region, which makes it is suitable for underground exploration robots. Seafloor explorations, in essence, could be realized by improving the gripping torque of the drilling robot and reducing its drilling torque. To resolve the problem, in this paper, three points were addressed. First, a setae-attached propulsion unit patterned to an earthworm structure was designed to attain an improved gripping torque for a subunit, typically at 30 kPa, by 1.7 times compared to that without setae. Second, the drilling resistance was reduced by the adjustment of the penetration and rotational speeds of the drilling robot based on the drilling properties of underwater ground. Lastly, the shape of the earth auger was considered for the reduction of the drilling torque. Following these solutions, the developed robot succeeded in drilling 430 mm into an underwater soil.

INDEX TERMS Drilling robot, underwater excavation, earthworm, seafloor exploration, marine robotics.

I. INTRODUCTION

Seabed mineral deposits, including rare earth elements, were found on the bottom of the ocean [1]–[3]. Samples of these resources should be collected and analyzed prior to utilization [4], [5] as sampling generally provides substantial clarification on their make-up process and distribution. Fig. 1 illustrates a general sampling method (vertical drilling) for seafloor explorations, which is similar to the method used in geological boring surveys. Here, a pipe-shaped sampler, e.g., a gravity corer, is sent from the drillship to the seafloor to collect soil samples [6]–[9]. There are also seafloor drilling robots such as the MeBo [10]. These robots do not need to stretch the drill tool from the sea water surface. Through these methods, samples can be obtained continuously with no operational disruptions. Thus, it is useful for acquiring the geological profile in the vertical direction. Nonetheless, it is an inefficient approach for investigating deposits widely distributed in the horizontal direction, given that the sampling range is limited to the diameter of the pipe (approximately 100 mm). This issue is compensated in the present study with the development of a seafloor robotic explorer design especially aimed for horizontal excavation and collection of rare earth element samples. By convention, these elements get deposited 2–3 m beneath the deep sea floor [11]. Wide-scale area exploration is possible by deployment of multiple robots to autonomously search beneath the seabed.

Three types of drilling robots have been proposed: striking-penetration, screw, and bioinspired. The first classification includes PLUTO [12], MMUM [13], and Hammer-driven-type penetrator [14], which penetrate the ground with a striking force. Screw-type robots include the screw subsurface

The associate editor coordinating the review of this manuscript and approving it for publication was Hui Xie.

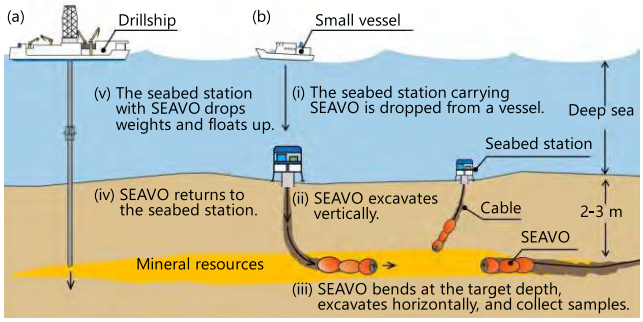

FIGURE 1. (a) General sampling method (vertical drilling). (b) Conceptual representation of SEAVO (horizontal drilling) as well as its future operation.

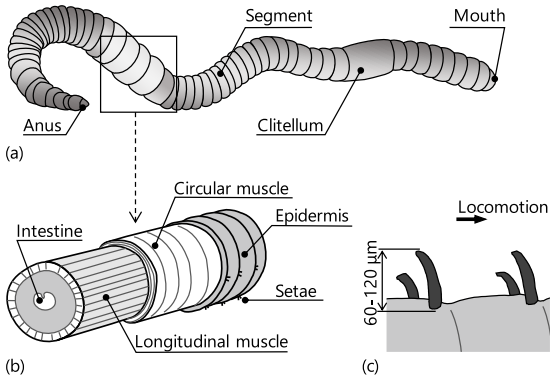

FIGURE 2. Typical earthworm structure. (a) An overview of the earthworm parts. (b) Parts of an earthworm. (c) Earthworm setae.

explorer [15], STSM [16], and DIGBOT [17], which excavate with low torque using a rotating screw. Bioinspired robots include IDDS [18] and IBR [19], which imitate an inchworm; RoboClam [20], which imitates a razor clam; and an actuated bivalve robot [21], which mimics a bivalve. However, these robots move in such a way that the side rubs with the borehole and dig with the soil pushed away as the drilled soils cannot be discharged out of the hole. As such, they become susceptible to earth pressure and cannot excavate deep underground.

These challenges can be overcome by focusing on the locomotion of an earthworm [22], [23] because it is only marginally susceptible to earth pressure [24]. In a previous study, we developed a drilling robot named SEAVO, mainly based on earthworm locomotion, and succeeded in excavating a depth of 613 mm at a turning radius of 1670 mm on land [25]. However, our attempt for underwater excavation was not successful.

In this paper, we introduce a vertical-type underwater drilling robot named SEAVO II and discuss the elements and techniques necessary for the realization of a seafloor robotic explorer. Specifically, SEAVO II is designed to support the reaction torque to the body (drilling torque) by the frictional force (gripping torque) acting between the borehole and the robot. In an underwater case, we are concerned with the challenge at which SEAVO II cannot support the drilling torque and becomes unable to excavate because of slipping. Therefore, our interest to realize underwater drilling is stressed on three key points, as follows:

(1) Development of a mechanism to improve the gripping torque (Section III).
(2) Study of drilling resistance reduction based on the drilling properties of underwater ground (Section IV).
(3) Consideration of the earth auger shape for reducing the drilling torque (Section V).

The future operation of SEAVO is described on the right side of Fig. 1. The operational process is divided into five phases: (i) The seabed station carrying SEAVO is dropped from a vessel. Such station is the mother unit and includes a power source for the robot and equipment operation. (ii) SEAVO performs a vertical excavation from the seabed station to the target depth (2–3 m). (iii) SEAVO bends at the target depth, conducts a horizontal excavation, and collects samples inside into its body. (iv) SEAVO returns to the seabed station. (v) The seabed station with SEAVO drops weights and floats up. For the purpose of this paper, we focus on phase (ii) and provide a discussion of the vertical excavation process while the robot is under water.

Accordingly, the paper is organized as follows. Section II presents a description of SEAVO II, whereas Section III introduces the developed setae-attached propulsion unit as a mechanism for improving the gripping torque. Section IV discusses the determination of the rotational and penetration speed of SEAVO II contributing to the reduction of the drilling resistance. Section V describes the shape of the earth auger considered for the purpose of reducing the drilling torque. In Section VI, the mechanisms and conditions developed under Sections III, IV, and V are applied on SEAVO II and then evaluated via underwater drilling experiments. Finally, Section VII presents a summary of the main findings and the future research direction.

II. SEAVO II CONCEPT

A. EARTHWORM LOCOMOTION

A typical earthworm structure is displayed in Fig. 2(a) and Fig. 2(b), with the mouth, clitellum, numerous segments divided by septa, a coelom containing the alimentary canal and nerve circuits, and the anus. In reference to Fig. 2(b), the inner wall of the body is composed of two muscle layers: a longitudinal muscle layer on the inside and a circular muscle layer on the outside. When the longitudinal muscle contracts in the axial direction, the segment gets thicker and shorter. When the circular muscle is actuated in a radial direction, the segment becomes thinner and extends in the axial direction. Fig. 2(c) shows all segments, excluding the first, which consist of setae (retractable bristles) that help the earthworm grip surfaces as it moves [26], [27].

The locomotion pattern of the earthworm is shown in Fig. 3. Earthworms nourish their bodies daily with organic matter and soil, and creates a space for their locomotion. An earthworm moves by propagating a retrograde peristalsis wave from the anterior part to the posterior region by muscle

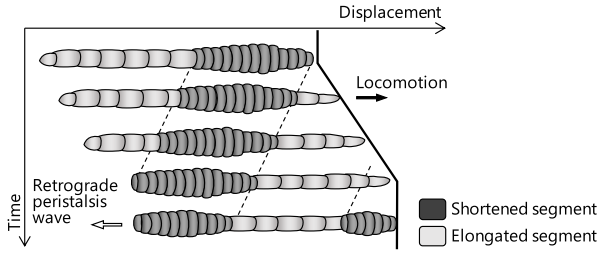

FIGURE 3. An actual earthworm locomotion pattern. Segments get shortened because of contraction by the longitudinal muscles, and segments elongate by actuation of the circular muscles.

contraction in the consecutive segments. Such locomotion manner is described in detail as follows:

(1) Longitudinal muscles provide contraction of the earthworm's shortened segments. During locomotion, thicker segments come in contact with the surface, and the friction created between the shortened segments and the ground increases.

(2) The elongated segments extend in the axial direction through the circular muscles. Reduced friction between the elongated segments and the moving surface keeps the smooth movement of the segments. Furthermore, the elongated segments can move forward as the shortened segments maintain contact with the surface.

(3) There are three advantages for such locomotion pattern: (a) It requires less space than other locomotion types, e.g., bipedal-based, wheel-based, or meandering locomotion. (b) It is expected to provide stability on irregular ground and inside a narrow pipe. (c) The earthworm becomes less susceptible to earth pressure. This pattern is deemed suitable not only for rescue robots but also for underground exploration and automatic endoscopic robots. Some robotic and biological engineering studies have recently investigated a peristaltic crawling robot based on the earthworm locomotion [28]–[30]. Similarly, various actuation methods have been studied to achieve this locomotion pattern [26], [31]–[39].

B. SEAVO II DRILLING ROBOT

Fig. 4 shows the conceptual model of SEAVO II, consisting mainly of an excavation unit and a propulsion unit. The former is aimed for ground excavation and for creating a space for locomotion, as in earthworms, whereas the latter is designed to move by extending and contracting cylinders to achieve the peristaltic movement of an earthworm [40], [41].

1) EXCAVATION UNIT

As the excavation unit is principally designed for ground excavation, for discharging of drilled soil from the outlet, and for securing a space for an earthworm-like propulsion, it consists of a motor (RS-775GM504, Suzakugiken), the waterproof case for the motor, a discharging outlet, a casing pipe, an earth auger, and a head part, as systematically illustrated in Fig. 5(a). The earth auger is displayed in Fig. 5(b). Configuration-wise, the auger head excavates the ground,

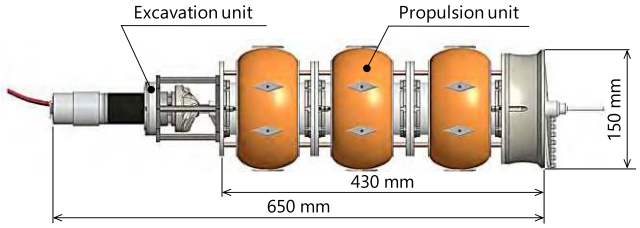

FIGURE 4. Conceptual model of SEAVO II with its excavation and propulsion units.

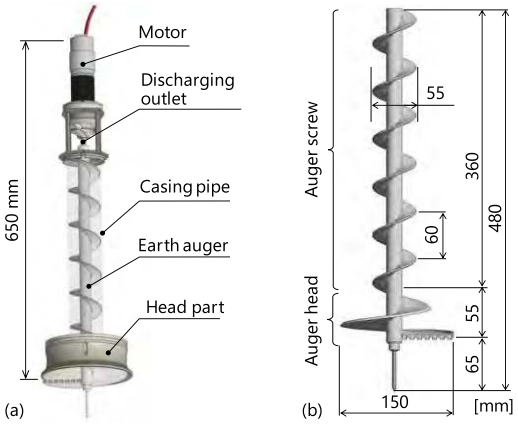

FIGURE 5. (a) Schematic diagram of the excavation unit. (b) Schematic diagram of the earth auger.

the auger screw conveys and discharges the drilled soil, and both have different diameters. Given this difference, the pitch of the head part is shortened to make the amount of soil moved per revolution equal in the auger head and each section of pitch length in the auger screw [23]. Section V considers the tip shape of the earth auger to reduce drilling resistance.

2) PROPULSION UNIT

The propulsion unit moves in a similar manner as an earthworm. The propulsion unit and its internal structures are shown in Fig. 6(a) and Fig. 6(b). The propulsion unit is patterned before the main parts of an earthworm, and the subunits correspond to an earthworm's segments. On one hand, the propulsion unit contains a hollow structure through which the drilled soil passes. On the other hand, the propulsion subunit consists of setae (described in Section III), plates, a casing pipe, guide shafts, a pneumatic cylinder (CJ2B16-15Z, SMC), and a rubber tube. These setae are part of the mechanism for the improvement of the gripping force [40], [41]. Air pressure causes the expansion of the rubber tube, which slides 10 mm by extending and contracting the cylinder. Pneumatic actuators are currently applied for such activity, but for deep sea applications, hydraulic actuators are future implementations. In order to realize neutral buoyancy, we are planning to use a buoyant material on SEAVO II and to study a drilling method that does not depend on its own weight. Moreover, because SEAVO II can be propelled only by the propulsive force of cylinders, it can assume vertically upward and horizontal movements.

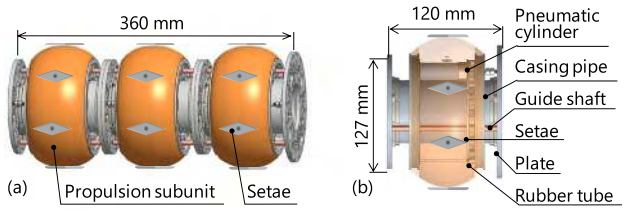

FIGURE 6. (a) A schematic diagram of the propulsion unit in SEAVO II, mainly composed of three propulsion subunits. (b) Internal structure of the propulsion unit.

Various mechanisms have already been developed for mimicking the structure of earthworms, for instance, with PEW-RO using artificial muscles [35], an origami-inspired worm robot [26], [36], a mesh-body worm robot [37], [38], and a friction-controlled soft robot [39]. For this study, we reproduce earthworm locomotion using a rubber tube and a cylinder in consideration of a push force, dustproof method, control system, etc. In this study, we use three propulsion units because three is the minimal number of segments for achieving earthworm-like peristaltic locomotion. We have more choices on locomotion gaits with more segments, and more segments can increase the speed [42].

3) LOCOMOTION PRINCIPLE OF SEAVO II

Fig. 7 provides an explanatory diagram for SEAVO II locomotion in the following five steps. Each propulsion subunit is labeled as subunits 1, 2, and 3, starting from the top.

(1) Each expanded subunit maintains contact with the wall of the hole.
(2) Subunit 1 contracts and moves forward.
(3) Subunit 1 expands again. After that, subunit 2 contracts and moves forward.
(4) Subunit 2 expands again. Next, subunit 3 contracts.
(5) Subunits 1 and 2 move backward simultaneously. At this point, the robot body moves forward relative to its starting position.

Such locomotion approach entails three advantages, as follows: (a) SEAVO II can move with less susceptibility to earth pressure, as the gripped part reciprocates during contraction. (b) SEAVO II operation is not dependent on its weight (gravitational force), and it advances using the propulsive force of cylinders. (c) SEAVO II does not need to push the soil away while excavating, and it can just expel the drilled soil out of the outlet.

III. SETAE-ATTACHED PROPULSION UNIT AS MECHANISM FOR IMPROVING THE GRIPPING TORQUE

The proposed setae-attached propulsion unit is patterned to the earthworm setae as a mechanism for improving the gripping torque. Such mechanism is necessary because underwater excavation using SEAVO II has yet to be realized at the present. As SEAVO II excavates the ground, the reaction torque to the body (drilling torque) needs the support of the

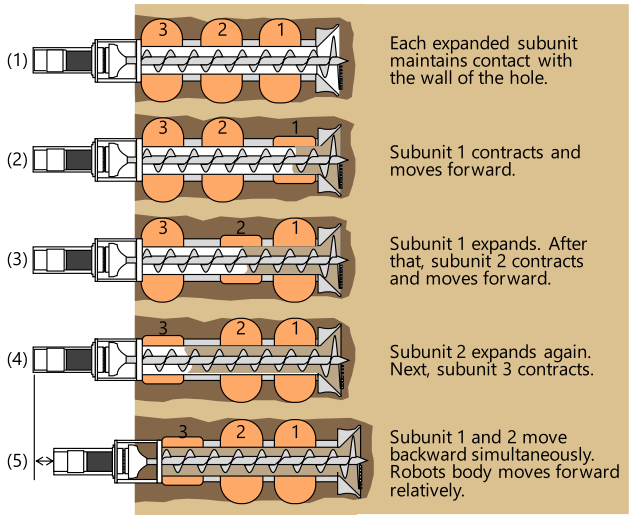

FIGURE 7. Locomotion principle of SEAVO II. A depth of 10 mm is propelled every 75 s by pattern repetition.

frictional force (gripping torque) acting between the drilling hole and the robot. In underwater environments, we are concerned on the possibility that SEAVO II may be unable to provide sufficient support to the drilling torque and therefore may not excavate because of ground fluidization. By fact, the gripping torque in an underwater environment is 72.9% lower than that in land and is less than the drilling torque [43]. A gripping torque that is lower than the drilling torque induces the rotation of the main body, in which SEAVO II would fall into a ''propulsion impossible'' state. Therefore, it is fundamentally necessary to improve the gripping torque for underwater excavation. This section highlights the description of the setae-attached propulsion unit designed to improve the propulsion ability of SEAVO II.

A. SETAE-ATTACHED PROPULSION UNIT

In reference to the earthworm parts depicted in Fig. 2, the locomotion and burrowing efficiency of the drilling robot is improved by the addition of bristles called setae on the segment surface. The setae can stretch out as the segment is radially expanded to increase the resistance force or form a temporary anchorage between the segment and the environment. In addition, the setae exhibit a slippery characteristic along the propulsion direction, which is less slippery in the reverse direction. On this account, the setae are useful for preventing slippage during movement [39]–[41], [44]–[46]. We consider these facts for the configuration design of the setae-attached propulsion unit.

A prototype of the propulsion subunit is shown in Fig. 8. In Fig. 9(a), the setae are spread passively by expansion of the subunit, which increases friction with surroundings, as anchors. Nevertheless, during contraction of the subunit, these setae are in close contact with the surface of the subunit and have little influence on the surroundings, a new mechanism that is expected to improve the gripping torque of the subunit. The material, shape, and mounting position

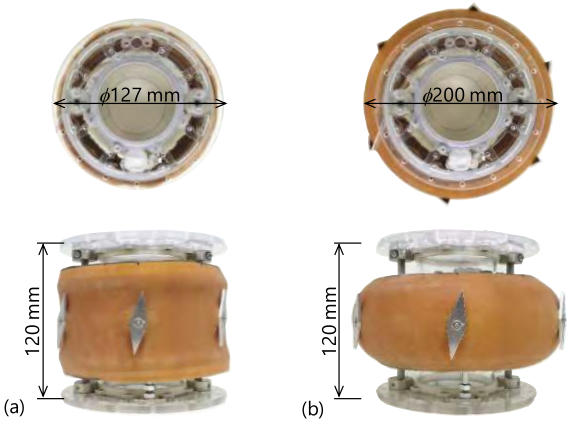

FIGURE 8. Actual appearance of the setae-attached propulsion subunit. (a) An unpressurized propulsion subunit. (b) Pressurized with 30 kPa.

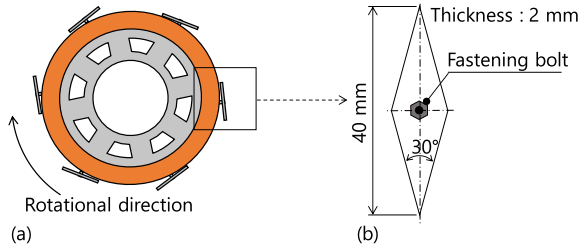

FIGURE 9. Gripping mechanism of the setae-attached propulsion subunit. (a) Setae spread by expansion of the subunit and increase in friction with surroundings, as anchors. (b) Adopted setae shape.

of the setae are described as follows. The setae material is made of cut-out 2-mm aluminum plates (A 2017) shaped into rhombus. A 2017 is the material used experimentally herein, but a future consideration is expected to be carried out with an aluminum plate (A5052), which is characterized by high resistance to seawater. For the shape, aside from rhombus, as shown in Fig. 9(b), other shapes are considered, for instance, circular or rectangular. Rhombus was the shape adopted as it exhibits small resistance during contraction and propulsion and can potentially improve the gripping torque. Regarding the position where the setae are attached, the actual location in earthworms is considered, that is, in the forward part of each segment, as illustrated in Fig. 2(c). On the contrary, because earthworms are faced with the difficulty to move backward with this structure, the setae in SEAVO II is attached at the middle part of the propulsion unit, as shown in Fig. 8, to enable the forward and backward drilling movements [40], [41].

B. EXPERIMENTAL STUDY ON THE CHARACTERISTICS OF THE SETAE-ATTACHED PROPULSION UNIT

We conducted experiments examining the characteristics of the setae-attached propulsion unit and verifying the influence of the number of setae on the gripping torque.

Let us first describe the target value of the gripping torque. A gripping torque that falls below the drilling torque value leads to the inability of SEAVO II to perform excavations by slipping. We confirmed that the rotation of the earth auger

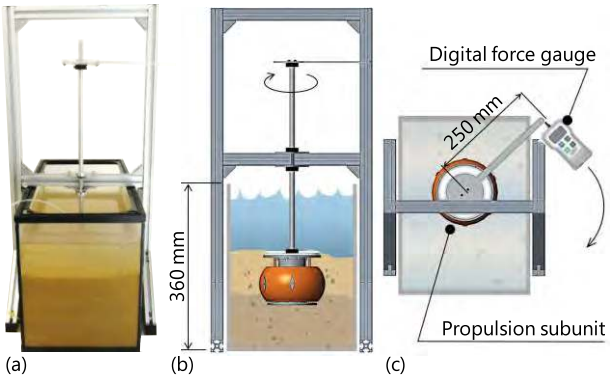

FIGURE 10. Experimental setup in measuring the gripping torque. (a) Picture of the setup. (b) Front view. (c) Top view.

at 20 rpm generates a drilling torque of up to 8.8 N m, according to experiments assessing the rotational speed characteristics of the robot (Section IV.C.1) in the simulated ground. For this simulation experiment, Toyoura sand was used as the sediment. The experimental process and details of Toyoura sand are described in Section IV.B.1. Two propulsion subunits were always inflated to support the excavation, by gripping of the wall surface, as illustrated in Fig. 7. In other words, a gripping torque of at least 4.4 N m was required for each propulsion subunit. On the basis of these conditions, the target gripping torque of the propulsion subunit was set to 4.4 N m.

Fig. 10 shows the equipment used in the experiment, which is composed of the propulsion subunit, an aluminum frame, a digital force gauge (FGJN-50, SHIMPO), and 590-mm long, 300-mm wide, and 30-mm high simulated ground. As earlier stated, Toyoura sand (Toyoura Keiseki Kogyo Co., Ltd.) was used for the simulated sediment. The experimental process was performed as follows. First, the propulsion subunit was buried in the simulated ground, and then, air pressure was applied on the subunit. Next, a load was applied in the rotational direction. For this step, the load was measured using a digital force gauge as soon as the propulsion subunit started moving. We repeated the experiment three times and calculated the average value of the gripping torque in those instances. Moreover, three prototype units with zero, two, four, and six setae attached were fabricated to assess their characteristics.

C. RESULTS AND DISCUSSION

Fig. 11 provides a graphical illustration of the experimental results for each propulsion subunit. Here, the gripping torque of the propulsion subunit was confirmed to increase with the attached setae. With no setae, the maximum gripping torque was 3.5 N m, which was less than the target 4.4 N m, at a pressure of 30 kPa. Moreover, the maximum gripping torque for six attached setae was 5.8 N m at the same pressure condition. Compared with the value yielded for the subunit without setae, the gripping torque for six setae, for 30 kPa, improved by 1.7 times, achieving the target value.

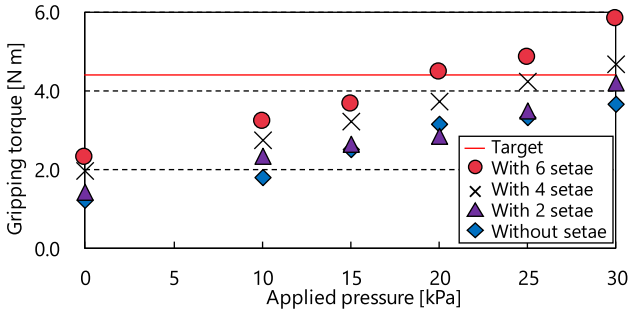

FIGURE 11. Relationship between applied pressure and gripping torque.

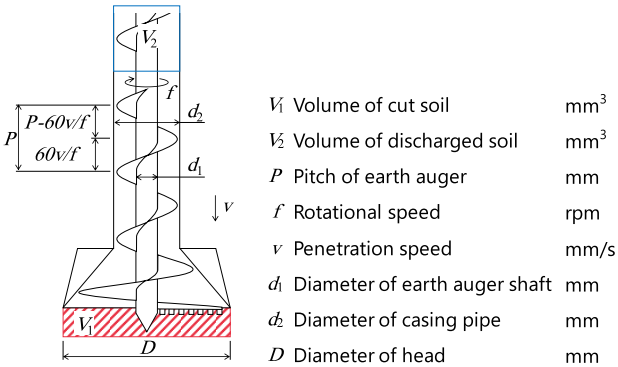

FIGURE 12. A model of the excavation unit during excavation.

In addition, the gripping torque was improved with more setae attached, by an average of approximately 0.35 N m per setae. As shown in Fig. 9(a), the setae attached to the propulsion subunit spread as the rubber tube expanded, along with an increase in the friction with the surroundings. Consequently, the gripping torque increased. More specifically, friction with the surroundings increased with increasing number of setae attached on the subunit. Similarly, the gripping torque at 0 kPa increased corresponding to the number of setae, although such increase was relatively small with respect to the gripping torque at the time of expansion. Thus, it was decided that the corresponding influence on the excavation operation was small. At an applied pressure of 20 kPa, the results with no bristles were 0.4 N m greater than those with two bristles. Such factor may be attributed to the fact that it was difficult to make the density of the underwater ground completely consistent in each measurement [41]. The above facts confirm the usefulness of the setae attached to the propulsion subunit, as detailed later in Section VI.

IV. REDUCTION OF DRILLING RESISTANCE BASED ON THE DRILLING PROPERTIES OF UNDERWATER GROUND

A large resistance is often times a serious problem in drilling. To improve the speed of SEAVO II, we reduced the drilling resistance. There were several methods proposed for drilling resistance reduction, including the application of water jetting, vibration, and telescopic motion. For the water jetting method, which is often used for the riser drilling system [43], [47], water or drilling mud is injected from the tip of the drill bit. The vibrational method has been proven effective for boring machines, whereas the telescopic motion method has been used for some digging robots, such as the RoboClam [20] and the Actuated Bivalve Robot [21]. These three methods are potentially effective in reducing the drilling resistance. However, applying these methods to SEAVO II requires mounting of new actuators on its body. This section introduces an alternative method of reducing the drilling resistance without the need to mount new actuators [48].

A. MODELING OF THE EXCAVATION UNIT DURING EXCAVATION

Fig. 12 shows a model of the excavation unit during excavation. For this section, the relationship between the penetration speed and the rotational speed was derived from the relationship between the cut soil and the discharged soil. Here, the volume of the cut soil was labeled as V_1, and the volume of the discharged soil was V_2. Soil density inside SEAVO II varies based on the relationship between V_1 and V_2 as follows:

(1) $V_1 > V_2$

Soil density inside SEAVO II increases when V_2 is less V_1. Further, the soil necessary for propulsion cannot be excavated and removed, and the ground is compressed. As a result, the drilling resistance increases, and the speed of SEAVO II decreases.

(2) $V_1 = V_2$

Under this condition, the space necessary for propulsion can be excavated, and the soil can be removed.

(3) $V_1 < V_2$

When V_2 exceeds V_1, the space required for propulsion can be excavated, and the soil can be removed. However, this is accompanied by an increase in friction due to the faster rotational speed.

First, we would like to determine the penetration speed v and the rotational speed f when $V_1 = V_2$, given the pitch of the earth auger P and penetration distance per revolution of the earth auger of $60v/f$. If the earth auger rotates n times as it penetrates to a predetermined depth, then V_1 is given by

$$V_1 = nLA\left(60\frac{v}{f}\right), \tag{1}$$

where L is the rate of change in the soil volume (the amount of soil after loosening/the amount of soil before loosening), A is the cross-sectional area of the head ($A = \pi D^2/4$), and D is the head diameter. Next, we consider the volume of the discharged soil. The height of rising soil after one rotation of the earth auger is given by $P- 60v/f$. Owing to friction, the soil discharge efficiency decreases. For simplicity, this factor was ignored here. Correspondingly, V_2 is expressed by

$$V_2 = nS\left(P - 60\frac{v}{f}\right), \tag{2}$$

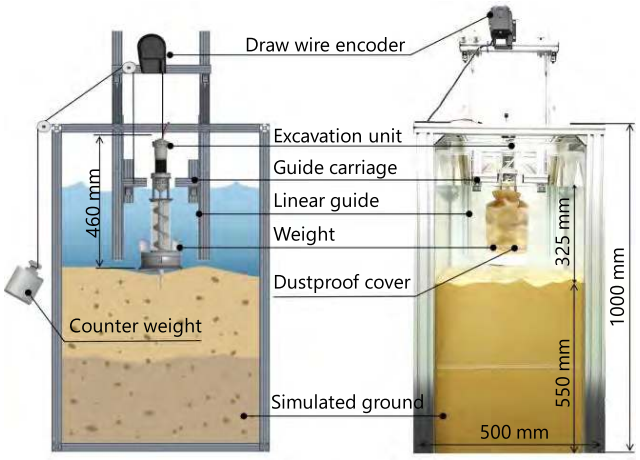

FIGURE 13. Experimental setup of the drilling properties.

where S is the effective cross-sectional area of the outlet ($S = \pi d_2^2/4 - \pi d_1^2/4$). Setting $V_1 = V_2$, we obtain

$$f = 60v\left(\frac{LA + S}{SP}\right). \tag{3}$$

In summary, Eq. (3) shows a simple relationship between the rotational speed and the penetration speed assuming $V_1 = V_2$ and is a useful equation when selecting the suitable rotational and penetration speeds for reducing the drilling resistance. On the contrary, this model does not consider the complex soil behavior, which led us to conduct two experiments: one for clarifying the difference of the drilling properties between the dried ground and the underwater ground, and another for investigating the drilling properties by the difference of the rotational speeds in the underwater ground. The validity of the model is discussed alongside a comparison between the results of these experiments [48].

B. DIFFERENCE IN DRILLING PROPERTIES BETWEEN DRY AND UNDERWATER GROUND

The drilling properties of underwater ground are clarified under this section in terms of a comparison of the differences in the drilling torque for land drilling against that of underwater. Consequently, we use the results to describe the relationship between the penetration speed and the drilling resistance for underwater drilling.

1) EXPERIMENTAL STUDY ON THE DRILLING PROPERTIES

We aimed to experimentally clarify the drilling properties of underwater ground because of its complex behavior, which makes theoretical analysis difficult. Fig. 13 illustrates the experimental setup, which consists of an excavation unit, linear guides, guide carriages, simulated ground, a draw wire encoder (D-1000Z-V, MUTOH), weights, and a counterweight. The excavation unit was fixed to the aluminum frame to ensure that it will not rotate, and it moved in the vertical direction along the slide rail. The counterweight was applied to stop the activity of the excavation unit. Without it, the excavation unit would descend because of its own weight. During the experiment, the excavation unit was propelled 10 mm every 75 s by lifting the counterweight. Such movement pattern was equivalent to the locomotion of SEAVO II, as shown in Fig. 7. The weight was mounted on the drilling unit to make the propulsive force of SEAVO II and that of the excavation unit used in this experiment coincide. SEAVO II advanced while pressing the ground by the cylinder force, which was measured using a force gauge to be 82 N. Meanwhile, the propulsive force of the excavation unit in this experiment coincided to the weight of the excavation unit. Therefore, both weights were attached to the excavation unit to provide drilling loads equivalent to the propulsive force (82 N) of SEAVO II. Moreover, the earth auger was rotated at 10 rpm. To ascertain the drilling resistance, we calculated the drilling torque from the current value of the motor (RS-775GM504, Suzakugiken) and measured the excavation depth using the draw wire encoder.

TABLE 1. Composition of the toyoura sand.

Chemical composition (Approx.)	Soil particle density	Mean particle size
SiO_2 : 92.6 %		
Al_2O_3 : 3.7 %		
Fe_2O_3 : 0.7 %	2.63 g/cm^3	0.21 mm
CaO : 0.5 %		
MgO : 0.2 %		

The simulated ground represented the surface layer of a seafloor. An actual seafloor contains various materials such as sand, mud, and plankton carcasses. Therefore, reproduction was difficult with the diversity and unevenness of marine sediments. On such consideration, we experimentally selected Toyoura sands (Toyoura Keiseki Kogyo Co., Ltd.), a main component of the marine sediment of uniform granularity, from the viewpoint of reproducibility of the experiment. The basic compositions of the Toyoura sand are listed in Table 1. The sediments were considered to have uniform deposition because the deep tide current was very slow, at approximately 3.6 mph. In detail, the simulated ground was produced following this procedure. A tank was first filled with a certain amount of tap water, and then, the sand was scattered in small amounts from the top and deposited uniformly in the tank up to a height of 550 mm. Dimension-wise, the tank was 500-mm long, 500-mm wide, and 1000-mm high. In the water saturated sediment, the volume of the contained moisture corresponded to the pore volume of the deposit. Therefore, its porosity could be calculated from the pore volume, which was 40%. We presumed that water pressure had no influence on the seafloor soils because it acted isotropically on the sand particle. On the basis of Eqs. (4), (5), and (6), it was clear that, regardless of water depth, the effective stress acting on the sand particles did not change. The total stress σ in the underwater ground is given as [49], [50]

$$\sigma = \sigma' + u, \tag{4}$$

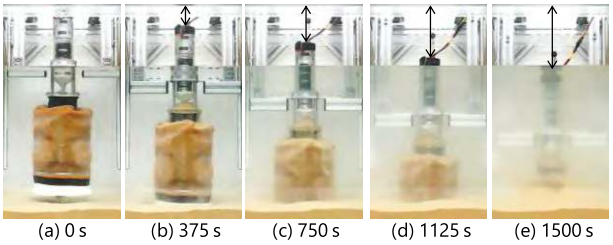

FIGURE 14. Time-lapse photos for the actual experiment.

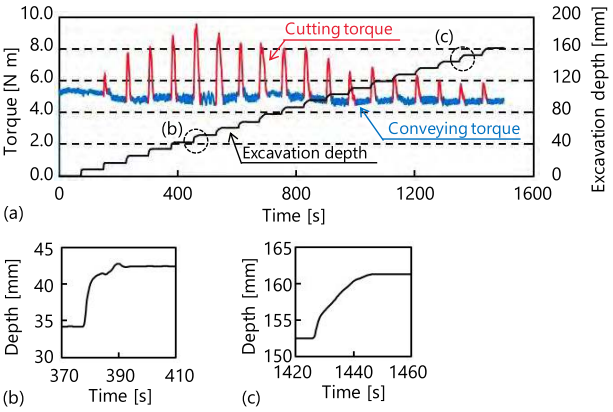

FIGURE 15. (a) Relationship between torque and excavation depth (submerged soil). (b) Excavation depth at 380 s. (c) Excavation depth at 1440 s.

where σ' is the effective stress and u is the pore water pressure expressed by

$$\sigma' = \rho_s g z, \tag{5}$$

$$u = \rho_w g (h + z), \tag{6}$$

where ρ_s is the density of sand, ρ_w is the density of water, g is gravitational acceleration, z is ground depth, and h is sea depth. The effective stress is the only effective factor for ground deformation [51], [52]; thus, water pressure would have no influence on the seafloor soil.

2) DIFFERENCE IN DRILLING PROPERTIES BETWEEN DRY AND UNDERWATER GROUND

Fig. 14 displays time-lapse photos of the experiment. After 247 s, the excavation unit discharged the drilled soil from the outlet part, and the drilled soil was deposited around the penetration area. We ended the experiment at 1500 s when the excavation unit reached the lowest end of its movable range. The results of the drilling torque and the excavation depth in the submerged ground are shown in Fig. 15. There were two types of drilling torque: the cutting torque and the conveying torque. The cutting torque was generated at regular intervals, the timing of which was coincident with the time the excavation depth increased. Consequently, the cutting torque existed once the ground was cut with the earth auger, whereas the conveying torque (between the cutting torques) occurred once the drilled soils were conveyed away.

The experimental results of the drilling torque in both submerged and dried ground are shown in Fig. 16. The cutting

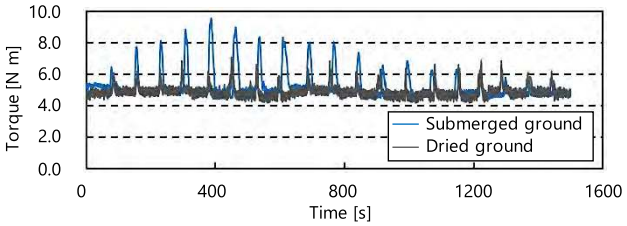

FIGURE 16. Experimental torque results (submerged and dried soils).

torque gradually increased from the start and then decreased after 463 s. On the contrary, the cutting torque in the dried ground did not change. The associated increase in the cutting torque of the submerged ground surface layer was due to its large moisture content and the fast initial penetration speed of the excavation unit, as a consequence of the loose ground. As shown in Fig. 15 (b), the excavation unit at the maximum drilling torque point descended in 10 s. Moreover, the penetration speed decreased as the ground became harder with depth, or rather generally, the penetration speed decreased with excavation depth, as depicted in Fig. 15 (c). In Fig. 15 (c), the excavation unit descended in 20 s. A few factors were involved in the variation of the drilling torque relative to the penetration speed. For instance, shear stress was generated in the submerged ground as the excavation proceeded. Conversely, the volume of the submerged ground expanded because of this shear stress, which is essentially described as the phenomenon of dilatancy. Dilatancy causes internal forces to agglomerate the sand particles, causing pore water pressure on the ground to decrease. At low penetration speed, the surrounding water intrudes, and the pore water pressure immediately returns to the original state. By contrast, when the penetration speed is fast, the water supply cannot intrude, and the pore water pressure remains low. When the second case occurs, both the shear and drilling resistances increase because of the associated increase in effective stress [53]–[55].

In general, the submerged ground is characterized by dilatancy, which further causes penetration speed to greatly affect the drilling resistance. For this reason, the slow penetration speed of SEAVO II effectively reduces the drilling resistance [48].

C. DRILLING PROPERTIES CAUSED BY THE DIFFERENCE IN ROTATIONAL SPEED

This section provides a discussion on rotational speeds that can be applied for efficient underground excavation with the drilling robot. We show a derived equation manifesting the relationship between the rotational speed and the penetration speed, which may be useful for reducing the drilling resistance. The experimental setup is similar to that described in Section IV.B.1.

1) RESULTS AND DISCUSSION

Experiments for this activity were carried out in submerged ground under four rotational speed conditions, namely, 10, 20, 30, and 40 rpm. The results are shown in Fig. 17.

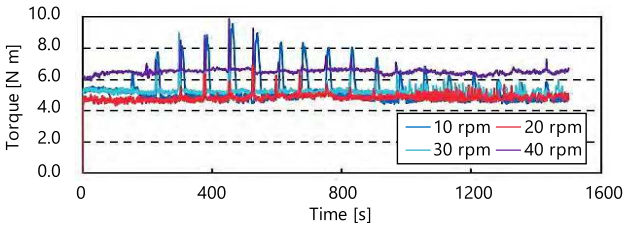

FIGURE 17. Torque at varying rotational speed (10, 20, 30, and 40 rpm).

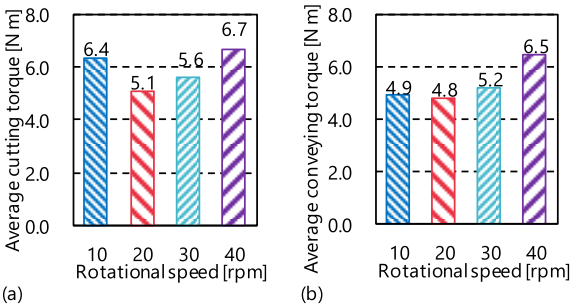

FIGURE 18. Average torque. (a) Average cutting torque and (b) average conveying torque at varying rotational speeds.

For each rotational speed, the drilling torque was divided into the cutting torque and the conveying torque, and the average value of each was calculated. Fig. 18(a) and Fig. 18(b) display the average cutting and conveying torques, respectively. Here, the average cutting torque initially decreased and then increased with faster rotational speed. At 20 rpm, the average cutting torque achieved a minimum value. Its value at 10 rpm was larger than that at 20 rpm because of the following. Basically, the amount of soil cut by the earth auger head and taken into the robot body is referred to as the cut soil, and the amount of soil discharged by the earth auger screw is defined as the discharged soil. At low rotational speed, the discharged soil per unit time would decrease, whereas the cut soil per unit time would depend on the penetration speed of SEAVO II. Thus, the amount of discharged soil would be less than the amount of cut soil. In such case, the density of the soil inside SEAVO II would increase. Further, the soil necessary for propulsion could not be excavated nor removed, leading to the ground being compressed. Consequently, the drilling resistance and drilling torque would increase. At a rotational speed faster than 20 rpm, the average cutting torque would increase because of increased friction buildup following the increase in rotational speed. Similarly, the average conveying torque would increase.

2) THEORETICAL VALUE OF PARAMETERS

We substituted the values of the parameters from the above experiment into Eq. (3) to obtain the theoretical value of rotational speed f. The values of each parameter, defined as in the previous sections, were as follows: $L = 1.1$ mm, $D = 150$ mm, $A = 17.7 \times 10^3$ mm^2, $d_1 = 20$ mm, $d_2 = 60$ mm, $S = 2.5 \times 10^3$ mm^2, $P = 60$ mm, and

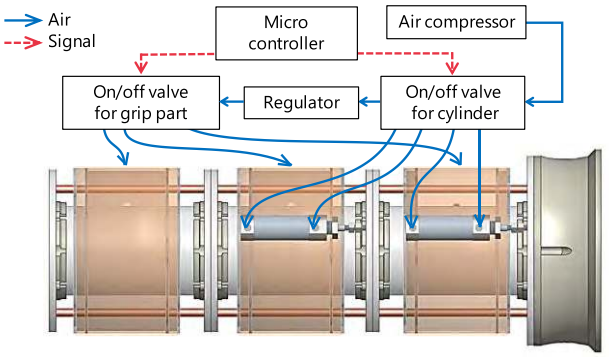

FIGURE 19. The SEAVO II system.

$v = 2.6$ mm/s. L is the value used in the sandy ground, and v is the average value calculated from the result of the excavation depth. Substituting these parameters into Eq. (3) produced a rotational speed of 23 rpm. Moreover, the experimental results showed that the drilling torque was lowest at 20 rpm, which justifies Eq. (3). In summary, Eq. (3) reflects a simple relationship between the rotational speed and the penetration speed, assuming that $V_1 = V_2$. This equation is useful when selecting the appropriate rotational and penetration speeds for the reduction of the drilling resistance [45].

D. ROTATIONAL AND PENETRATION SPEED REQUIREMENT FOR SEAVO II

We specified the required rotational and penetration speeds of SEAVO II based on the combined results of Sections IV.A, IV.B, and IV.C. As mentioned in Section IV.B, low penetration speed suppresses dilatancy and helps in reducing drilling resistance. As for the other two sections, it is implied that drilling can be performed most efficiently considering a rotational speed of 20 rpm, which is our reason for setting the rotational speed of the robot to this value. Substituting 20 rpm in Eq. (3) yields a penetration speed of 2.3 mm/s, which should be maintained until drilling completion. However, the current penetration speed of SEAVO II is 6.8 mm/s because of the instantaneously pressurized cylinder. This value is too fast. This section describes a control mechanism for controlling such excessive penetration speed. Fig. 19 addresses the control system of SEAVO II. Here, air is supplied by the compressor, and expansion and contraction of the rubber tube and the cylinder are controlled by an on–off valve (V100-1-6, SMC). Each on–off valve is controlled via a microcomputer (Arduino). In addition, there is a difference in applied pressure for the rubber tube (30 kPa) and the cylinder (200 kPa) so that such was adjusted via a regulator. To suppress the penetration speed, we controlled the on–off valve (V100-1-6, SMC) via a microcomputer (Arduino) and pressurized the air to the cylinder in a stepwise manner. The difference in the propulsive distance SEAVO II travels between the stepwise air application ($v = 2.3$ mm/s) and instantaneous air application ($v = 6.8$ mm/s) is shown in Fig. 20, and the usefulness of these conditions is confirmed in Section VI.

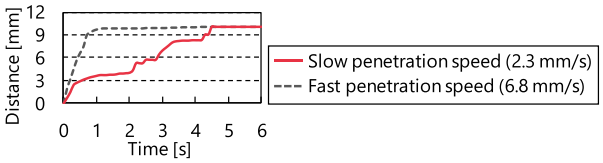

FIGURE 20. Propulsion distance of SEAVO II under slow and fast penetration speeds.

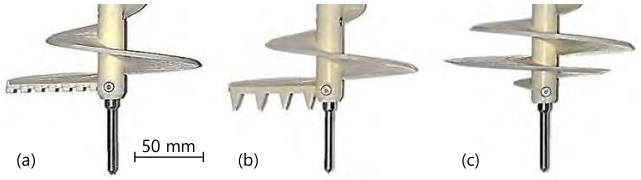

FIGURE 21. Head part of the earth auger. (a) Flat-tip type (previous type). (b) Rake type has bits larger than those of (a). (c) Cone-tip type.

V. CONE-TIP-TYPE EARTH AUGER AS A MECHANISM OF DRILLING TORQUE REDUCTION

An earth auger rotating in the soil receives a corresponding drilling torque from the soil. On such basis, a large drilling torque generated by the system becomes a serious problem. During propulsion, the soil in front of SEAVO II was compressed, leading to instantaneous generation of a large cutting torque. Such cutting torque should be lessened to loosen the front ground. This section presents the suitable earth auger shape to aid in the reduction of the drilling resistance. In particular, two new kinds of earth auger with stirring function, namely, cone-tip type and rake type, are proposed, in consideration of their relative performance [43].

A. CONE-TIP-TYPE AND RAKE-TYPE EARTH AUGERS

Flat-tip-type (previous type), rake-type, and cone-tip-type earth augers are displayed in Fig. 21(a), Fig. 21(b), and Fig. 21(c), respectively. By function, the rake type enlarges the earth auger a bit to loosen the soil, whereas the cone-tip type, owing to its conical shape, helps in reducing the penetration resistance. Further, the screw part of the tip of the cone type loosens the soil to reduce the drilling torque. We tested the drilling performance of these earth augers to validate their usefulness, following the same experimental setup as that described in Section IV.B.1. Each earth auger was rotated at 10 rpm.

B. RESULTS AND DISCUSSION

The results for the drilling torque using the flat-tip-type and rake-type earth augers are shown in Fig. 22. For the latter, the conveying torque decreased, and the cutting torque increased. Reduction in the conveying torque was attributed to the loosened sand at the rake section, as well as the decrease in the density of the drilled soil. On the contrary, the cutting torque increased because of a larger area of the bits of the rake-type earth auger, as compared to the former. Specifically, the maximum drilling torque yield using the rake-type earth auger was 9.2 N m at 1139 s, and that for the flat-tip type was 9.6 N m at 463 s.

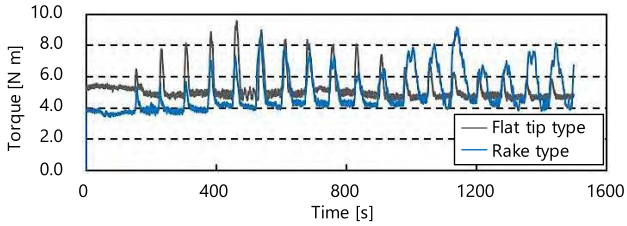

FIGURE 22. Comparison of torque results for flat-tip-type and rake-type earth augers.

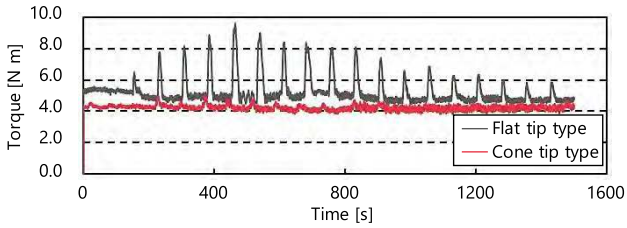

FIGURE 23. Comparison of torque results for flat-tip-type and cone-tip-type earth augers.

TABLE 2. Experimental contents of SEAVO II excavation.

	Penetration speed	Earth auger
Experiment 1	Fast (6.8 mm/s)	Flat tip type
Experiment 2	Slow (2.3 mm/s)	Flat tip type
Experiment 3	Slow (2.3 mm/s)	Cone tip type

Accordingly, the results for the drilling torque using the flat-tip-type and cone-tip-type earth augers are illustrated in Fig. 23. Here, both the cutting torque and conveying torque of the two earth augers decreased, the former being attributed to the loosened compression of the front ground by the conical tip. Moreover, cutting the ground by the screw contributed to a low torque. Meanwhile, the conveying torque declined because of the loosening of the drilled soil by the screw part. The maximum drilling torque yield by the cone-tip type earth auger was 5.0 N m at 371 s [43].

The results above confirm the usefulness of the cone-tip-type earth auger. Thus, we applied it on the system of SEAVO II in conducting the drilling experiments described in Section VI.

VI. DRILLING EXPERIMENTS WITH SEAVO II

We thus far confirmed the reasonable usefulness of the setae-attached propulsion unit, with the low penetration speed and cone-tip-type earth auger suggested by the drilling experiments in the previous section. Here, we compare the torque and the corresponding excavation depth after performing three kinds of experiments, as shown in Table 2. The setae-attached propulsion unit was mounted on the drilling robot for all experiments. Table 2 confirms the usefulness of low penetration speed in Experiment 2, as compared to Experiment 1, and Experiment 3 demonstrates the usefulness of the

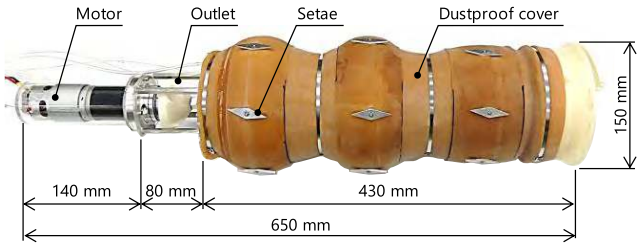

FIGURE 24. Dustproofed SEAVO II with setae.

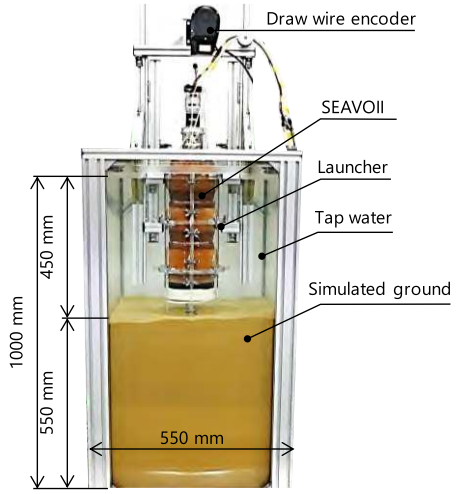

FIGURE 25. Experimental setup for the SEAVO II excavation.

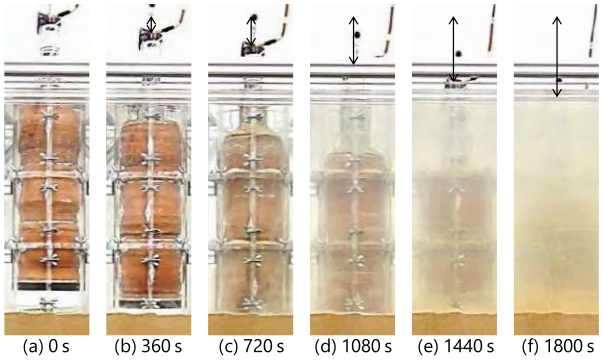

FIGURE 26. Time-lapse photos for SEAVO II excavation up to 1800 s.

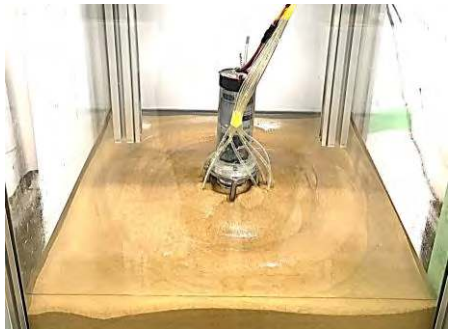

FIGURE 27. Post-experimental state after water is removed from the soil tank.

cone-tip-type earth auger, as compared to the flat-tip type in Experiment 2.

A. SEAVO II EXCAVATION EXPERIMENT

Fig. 24 presents an overview of the developed SEAVO II drilling robot, particularly covered with a rubber tube for dustproofing. The accompanying experimental setup is shown in Fig. 25, consisting of the SEAVO II equipment, a launcher, simulated ground, and a draw wire encoder (D-1000Z-V, MUTOH). The launcher served as a supporting frame for the robot. For this experiment, we compared the drilling torque and the completion time, measured the motor current, and calculated the drilling torque based on this current. Additionally, we measured the excavation depth using a draw wire encoder. The experiment was terminated once SEAVO II reached 430 mm because of limitations associated to the setup.

B. RESULTS AND DISCUSSION ON EXPERIMENT 1

We conducted Experiment 1 by installing a setae-attached propulsion unit on SEAVO II. Here, the penetration speed for the robot was 6.8 mm/s using a flat-tip-type earth auger. Fig. 26 shows the time-lapse photos of the SEAVO II excavation up to 1800 s, after which the inside of the aquarium became turbid because of the soil discharged from SEAVO II, which created a difficulty in visually confirming the measurement values. The discharge of soil from the outlet of SEAVO II was confirmed at 540 s. Further, SEAVO II reached 430 mm (the distance from the tip to the outlet) at 4686 s. Fig. 27 depicts the state when water in the soil tank was removed after the experiment. Notice that the entire robot has penetrated the ground. The torque and excavation depth results for SEAVO II under Experiment 1 are illustrated in Fig. 28. Apparently, a large drilling torque was generated at the surface from dilatancy, previously described in Section IV.B.2. With respect to the usefulness of the setae-attached propulsion unit, the results in Section III.C justified that the allowable torque that can be supported by two subunits without setae is 7.4 N m, and the allowable torque that can be supported by two setae-attached subunits is 11.6 N m. In Experiment 1, the maximum value of the torque was 10.5 N m at 1061 s, although several drilling torques above 7.6 N m were recorded. Thus, given the case where setae were not attached to SEAVO II, the robot would not excavate. Meanwhile, underwater drilling was successful after mounting the setae-attached propulsion unit. In particular, the completion time for excavating 430 mm was 4686 s, which was 1461 s slower than the expected completion time of 3225 s, presumably because SEAVO II is capable of self-propulsion by 10 mm every 75 s. With the slow completion time, the soil for discharge could not be excavated and removed as an activity to generate locomotion space because of an increase in the drilling resistance. As a consequence, the speed of SEAVO II decreased.

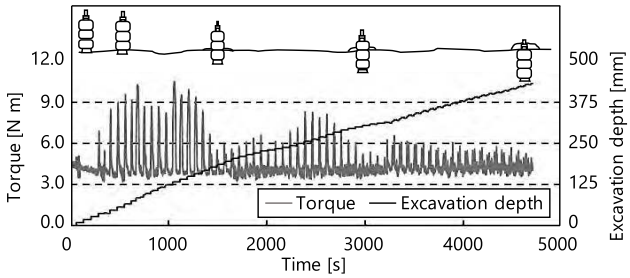

FIGURE 28. Torque and excavation depth results for Experiment 1.

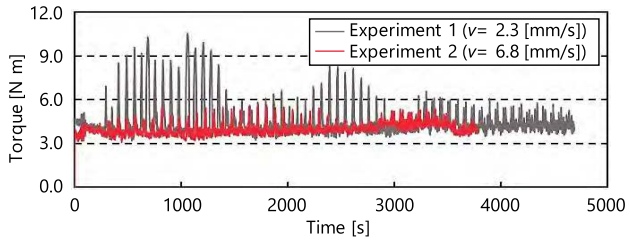

FIGURE 29. Comparison of torque results for Experiments 1 and 2.

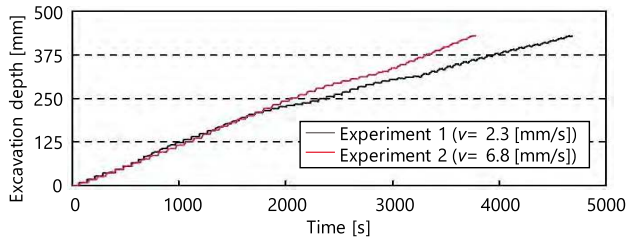

FIGURE 30. Comparison of torque results for experiments 1 and 2.

C. RESULTS AND DISCUSSION ON EXPERIMENT 2

We confirmed the usefulness of the conditions ($f = 20$ rpm and $v = 2.3$ mm/s) in Experiment 2. Fig. 29 and Fig. 30 show the drilling torque and excavation depth results of the entire experiment. Here, the cutting torque for the slow penetration speed was remarkably less than that for the fast penetration speed because dilatancy was suppressed by the low speed. In terms of excavation depth, the required completion time for fully excavating 430 mm was 4686 s in the case of the fast penetration speed ($v = 6.8$ mm/s), as compared to 3775 s in the case of the slow penetration speed ($v = 2.3$ mm/s). On average, the expected time of completion was 3225 s. This suggests that the speed of SEAVO II improved compared to the consideration of a fast penetration speed. Thus, the space necessary for the locomotion of the equipment could be excavated and removed through adjustment of the rotational speed and the penetration speed, in accordance with Eq. (3). Consequently, the speed of SEAVO II improved, which confirms the usefulness of low penetration speed.

D. RESULTS AND DISCUSSION ON EXPERIMENT 3

Experiment 3 confirms the usefulness of the cone-tip-type earth auger. The results for the drilling torque and excavation depth for this experiment are shown in Fig. 31 and Fig. 32, respectively. For the drilling torque, note that the cutting torque of the cone-tip-type earth auger was reduced, as compared to the flat-tip type. Additionally, the decrease in penetration resistance was believed to be attributed to the use of the cone-tip-type earth auger. For the excavation depth, the time required for drilling 430 mm was 3775 s (Experiment 2) for the flat-tip type and 3231 s for the cone-tip type. Thus, drilling speed improved compared to the former, which validates the usefulness of the cone-tip-type earth auger.

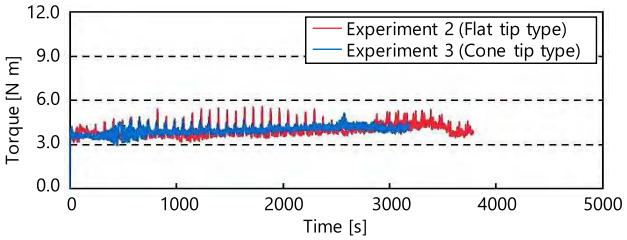

FIGURE 31. Comparison of torque results for experiments 2 and 3.

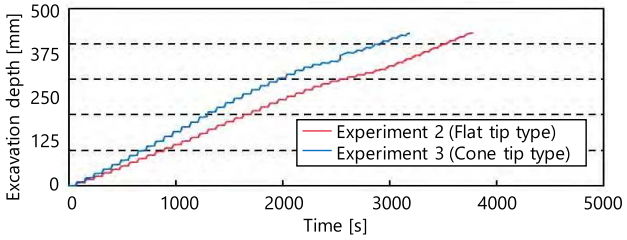

FIGURE 32. Comparison of excavation depth results for experiments 2 and 3.

VII. CONCLUSION AND FUTURE WORK

The main findings of the study can be generalized as follows:

- A setae-attached propulsion subunit patterned on the structural appearance of an earthworm was proposed for underwater excavation. We conducted experiments to validate the usefulness of the subunit in propulsion. Consequently, the gripping torque improved by 1.7 times with the attached setae.
- An equation showing the relationship between the rotational speed and the penetration speed was successfully derived and further employed to obtain reasonable conditions (penetration speed: 2.3 mm/s; rotational speed: 20 rpm) for efficiently reducing the drilling resistance.
- A cone-tip-type earth auger for the robot equipment was developed to aid in the reduction of the drilling torque. We successfully demonstrated its ability to reduce the drilling torque via experiments.
- Our proposed underwater drilling robot SEAVO II, equipped with a setae-attached propulsion unit, designed via consideration of the conditions of rotational and penetration speeds above, and mounted with a cone-tip-type earth auger, was the highlight of the study. We performed several underwater drilling experiments, which

confirmed the capability of SEAVO II to fully excavate a depth of 430 mm at 3231 s. The experiments likewise confirmed the usefulness of SEAVO II for seafloor excavations.

Note that we had to stop the experiment as soon as SEAVO II excavated a depth of 430 mm because of the limited size of the experimental equipment. Deeper than 430 mm, the discharging outlet would be buried, which makes discharging of the drilled soil impossible. Realizing this constraint, we are planning to formulate a new discharge mechanism to enable the smooth discharge of drilled soil by the proposed SEAVO II. This step would be complemented by shallow-area experiments in the ocean to assess the excavation feasibility for underwater ground depth beyond 430 mm. Additionally, we are planning to develop flexion joints for the robot to achieve directional drilling.

ACKNOWLEDGMENT

The authors would like to thank Enago (www.enago.jp) for the thorough editing assistance on the use of English language in the manuscript.

REFERENCES

[1] H. Nakajoh, H. Osawa, T. Miyazaki, K. Hirata, T. Sawa, and H. Utsugi, "Development of work class ROV applied for submarine resource exploration in JAMSTEC," in *Proc. IEEE Oceans*, May 2012, pp. 1–5. doi: 10.1109/OCEANS-Yeosu.2012.6263437.

[2] H. Yoshida, T. Hyakudome, S. Ishibashi, T. Sawa, Y. Nakano, H. Ochi, Y. Watanabe, T. Nakatani, Y. Ota, M. Sugesawa, and M. Matsuura, "An autonomous underwater vehicle with a canard rudder for underwater minerals exploration," in *Proc. IEEE Int. Conf. Mechatronics Autom.*, Aug. 2013, pp. 1571–1576.

[3] S. D. Scott, "Marine minerals: Their occurrences, exploration and exploitation," in *Proc. IEEE OCEANS*, Sep. 2011, pp. 1–8. doi: 10.23919/OCEANS.2011.6107119.

[4] H. Yoshida, T. Aoki, H. Osawa, S. Ishibashi, Y. Watanabe, J. Tahara, T. Miyazaki, and K. Itoh, "A deepest depth ROV for sediment sampling and its sea trial result," in *Proc. Symp. Underwater Technol. Workshop Sci. Submarine Cables Related Technol.*, Apr. 2007, pp. 28–33.

[5] X. Zhang, Z. Luan, J. Yan, and C. Chen, "Development of a deep-sea sediment long coring system based on a Jackhammer for R/V Kexue," in *Proc. IEEE Oceans*, Oct. 2012, pp. 1–6.

[6] K. Wada, "Coring technology to be applied in IODP NanTroSEIZE," in *Proc. OCEANS MTS/IEEE Kobe Techno-Ocean*, Apr. 2008, pp. 1–4. doi: 10.1109/OCEANSKOBE.2008.4531001.

[7] M. Kyo, "Challenges to drill through seismogenic zone," in *Proc. IEEE Int. Underwater Technol. Symp. (UT)*, Mar. 2013, pp. 1–7. doi: 10.1109/UT.2013.6519908.

[8] T. McGinnis, "Remote control seafloor coring in the west mariana basin," in *Proc. 21st Century OCEANS MTS/IEEE Riding Crest*, Sep. 1999, pp. 255–256.

[9] J. Liu, J. Chen, F. Liu, L. Gu, Y. Sheng, M. Zhang, D. Zheng, B. Xiao, X. Geng, and Z. Sha, "Development of one pressure core transfer device for one long gravity-piston pressure-retained corer," in *Proc. IEEE Oceans-St. John's*, Sep. 2014, pp. 1–6. doi: 10.1109/OCEANS.2014.7003018.

[10] T. Freudenthal and G. Wefer, "Shallow drilling in the deep sea: The sea floor drill rig MeBo," in *Proc. IEEE OCEANS*, May 2009, pp. 1–4. doi: 10.1109/OCEANSE.2009.5278133.

[11] Y. Kato, K. Fujinaga, K. Nakamura, Y. Takaya, K. Kitamura, J. Ohta, R. Toda, T. Nakashima, and H. Iwamori, "Deep-sea mud in the pacific ocean as a potential resource for rare-earth elements," *Nature Geosci.*, vol. 4, pp. 535–539, Jul. 2011.

[12] L. Richter, P. Coste, V. Gromov, and A. Grzesik, "The mole with sampling mechanism (MSM)—Technology development and payload of beagle 2 mars Lander," in *Proc. 8th ESA Workshop Adv. Space Technol. Robot. Autom.*, 2007, pp. 2–4.

[13] C. R. A. Stoker, A. Gonzales, and J. R. Zavaleta, "Moon/mars underground mole," in *Proc. NASA Sci. Technol. Conf.*, 2007, p. C10P1.

[14] Y. Shen, S. Jiang, C. Xu, W. Zhang, and X. Wu, "Study on Optimization of Structure Parameters to the Penetrator," in *Proc. IEEE Int. Conf. Mechatronics Autom.*, Aug. 2016, pp. 1518–1523.

[15] K. Nagaoka, T. Kubota, M. Otsuki, and S. Tanaka, "Robotic screw explorer for lunar subsurface investigation: Dynamics modelling and experimental validation," in *Proc. IEEE Int. Conf. Adv. Robot.*, Jun. 2009, pp. 1–6.

[16] S. Yasuda, K. Komatsu, and S. Tanaka, "Self-turning screw mechanism for burying geophysical sensors under regolith," in *Proc. Int. Symp. Artif. Intell., Robot. Automat. Space*, 2012, p. 09B02.

[17] R. Abe, Y. Kawamura, K. Kamijima, and K. Murakami, "Performance evaluation of contra-rotating drill for DIGBOT," in *Proc. SICE Annu. Conf.*, Aug. 2010, pp. 885–888.

[18] S. Rafeek, S. P. Gorevan, P. W. Bartlett, and K. Y. Kong, "The inchworm deep drilling system for kilometer scale subsurface exploration of europa (IDDS)," in *Forum on Innovative Approaches to Outer Planetary Exploration 2001–2020*. Jan. 2001, p. 68.

[19] Z. Weiwei, J. Shengyuan, S. Yi, L. Peng, and C. Huazhi, "Development of an inchworm-type drilling test-bed for planetary subsurface exploration and preliminary experiments," in *Proc. IEEE Int. Conf. Robot. Biomimetics*, Dec. 2016, pp. 2187–2191.

[20] A. G. Winter, R. L. H. Deits, D. S. Dorsch, A. E. Hosoi, and A. H. Slocum, "Teaching RoboClam to dig: The design, testing, and genetic algorithm optimization of a biomimetic robot," in *Proc. IEEE/RSJ Int. Conf. Intell. Robots Syst.*, Oct. 2010, pp. 4231–4235.

[21] A. Koller-Hodac, D. P. Germann, A. Gilgen, K. Dietrich, M. Hadorn, W. Schatz, and P. E. Hotz, "Actuated bivalve robot study of the burrowing locomotion in sediment," in *Proc. IEEE Int. Conf. Robot. Autom.*, May 2010, pp. 1209–1214.

[22] H. Omori, T. Hayakawa, and T. Nakamura, "Locomotion and turning patterns of a peristaltic crawling earthworm robot composed of flexible units," in *Proc. IEEE/RSJ Int. Conf. Intell. Robots Syst.*, Sep. 2008, pp. 1630–1635.

[23] H. Omori, T. Murakami, H. Nagai, T. Nakamura, and T. Kubota, "Planetary subsurface explorer robot with propulsion units for peristaltic crawling," in *Proc. IEEE Int. Conf. Robot. Autom.*, May 2011, pp. 649–654.

[24] R. M. Alexander, *Exploring Biomechanics: Animals in Motion*. New York, NY, USA: W.H. Freeman Company, 1992, pp. 77–79.

[25] N. Tadami, M. Nagai, T. Nakatake, A. Fujiwara, Y. Yamada, T. Nakamura, H. Yoshida, H. Sawada, and T. Kubota, "Curved excavation by a sub-seafloor excavation robot," in *Proc. Int. Conf. Intell. Robots Syst.*, Sep. 2017, pp. 4950–4956.

[26] H. Fang, Y. Zhang, and K. W. Wang, "Origami-based earthworm-like locomotion robots," *Biomimetics*, vol. 12, no. 6, 2017, Art. no. 065003.

[27] E. V. Mangan, D. A. Kingsley, R. D. Quinn, and H. J. Chiel, "Development of a peristaltic endoscope," in *Proc. IEEE Int. Conf. Robot. Autom.*, May 2002, pp. 347–352.

[28] A. Menciassi, S. Gorini, G. Pernorio, and P. Dario, "A SMA actuated artificial earthworm," in *Proc. IEEE Int. Conf. Robot. Autom. (ICRA)*, Apr./May 2004, pp. 3282–3287.

[29] J. Zuo, G. Yan, and Z. Gao, "A micro creeping robot for colonoscopy based on the earthworm," *J. Med. Eng. Technol.*, vol. 29, no. 1, pp. 1–7, 2005.

[30] B. Kim, M. G. Lee, Y. P. Lee, Y. Kim, and G. Lee, "An earthworm-like micro robot using shape memory alloy actuator," *Sens. Actuators A, Phys.*, vol. 125, no. 2, pp. 429–437, 2006.

[31] N. Saga and T. Nakamura, "A prototype of peristaltic robot using pneumatic artificial muscle," *Intell. Automat. Syst.*, vol. 8, no. 1, pp. 85–95, 2004.

[32] N. Saga and T. Nakamura, "Development of a peristaltic crawling robot using magnetic fluid on the basis of the locomotion mechanism of the earthworm," *Smart Mater. Struct.*, vol. 13, no. 3, pp. 85–95, 2004.

[33] T. Nakamura, T. Kato, T. Iwanaga, and Y. Muranaka, "Development of a peristaltic crawling robot using servomotors based on the locomotion mechanism of earthworms," in *Proc. IEEE Int. Conf. Robot. Autom.*, May 2006, pp. 4342–4344.

[34] T. Nakamura, T. Kato, T. Iwanaga, and Y. Muranaka, "Development of a peristaltic crawling robot based on earthworm locomotion," *J. Robot. Mechatronics* vol. 18, no. 3, pp. 299–304, 2006.

[35] Y. Mano, R. Ishikawa, Y. Yamada, and T. Nakamura, "Development of contraction force control system of peristaltic crawling robot for sewer pipe inspection," in *Proc. IEEE/ASME Int. Conf. Adv. Intell. Mechatronics (AIM)*, Jul. 2018, pp. 936–941.
[36] C. D. Onal, R. J. Wood, and D. Rus, "An origami-inspired approach to worm robots," *IEEE/ASME Trans. Mechatronics*, vol. 18, no. 2, pp. 430–438, Apr. 2013.
[37] Y. Huang, A. Kandhari, H. Chiel, R. Quinn, and K. Daltorio, "Slip reduction controls of mesh-body worm robot developed from a mathematical model," in *Proc. IEEE Int. Conf. Robot. Biomimetics (ROBIO)*, Dec. 2017, pp. 1474–1479.
[38] K. A. Daltorio, A. S. Boxerbaum, A. D. Horchler, K. M. Shaw, H. J. Chiel, and R. D. Quinn, "Efficient worm-like locomotion: Slip and control of soft-bodied peristaltic robots," *Bioinspiration Biomimetics*, vol. 8, no. 3, Sep. 2013, Art. no. 035003.
[39] J. Z. Ge, A. A. Calderón, L. Chang, and N. O. Pérez-Arancibia, "An earthworm-inspired friction-controlled soft robot capable of bidirectional locomotion," *Bioinspiration Biomimetics*, vol. 14, no. 3, Feb. 2019, Art. no. 036004.
[40] N. Tadami, K. Isak, T. Nakatake, A. Fujiwara, Y. Yamada, T. Nakamura, M. Sugesawa, and H. Yoshida, "Proposal of propulsion unit based on earthworm setae for underwater excavation robot," in *Proc. 21st Int. Conf. Climbing Walking Robots Support Technol. Mobile Mach.*, Sep. 2018, pp. 369–377.
[41] N. Tadami, K. Isaka, T. Nakatake, A. Tujiwara, Y. Yamada, T. Nakamura, M. Sugesawa, and H. Yoshida, "Underwater excavation by excavation robot equipped with propulsion unit based on earthworm setae," in *Proc. Int. Conf. Robot. Biomimetics (ROBIO)*, Dec. 2018, pp. 51–58. doi: 10.1109/ROBIO.2018.8664782.
[42] H. Fang, C. Wang, S. Li, K. W. Wang, and J. Xu, "A comprehensive study on the locomotion characteristics of a metameric earthworm-like robot: Part B: Gait analysis and experiments," *Multibody Syst. Dyn.*, vol. 35, no. 2, pp. 153–177, Oct. 2015.
[43] K. Isaka, N. Tadami, A. Fujiwara, T. Nakatake, M. Suzesawa, Y. Yamada, H. Yoshida, and T. Nakamura, "Water jetting excavation and consideration of earth auger shape to reduce drilling torque for seabed robotic explorer," in *Proc. IEEE/ASME Int. Conf. Adv. Intell. Mechatron.*, Jul. 2018, pp. 887–892.
[44] J. Kwon, S. Park, B. Kim, and J.-O. Park, "Bio-material property measurement system for locomotive mechanism in gastro-intestinal tract," in *Proc. IEEE Int. Conf. Robot. Autom.*, Apr. 2005, pp. 1303–1308.
[45] H. Fang, S. Li, K. W. Wang, and J. Xu, "Phase coordination and phase–velocity relationship in metameric robot locomotion," *Bioinspiration Biomimetics*, vol. 10, no. 6, Oct. 2015, Art. no. 066006.
[46] K. J. Quillin, "Kinematic scaling of locomotion by hydrostatic animals: Ontogeny of peristaltic crawling by the earthworm lumbricus terrestris," *J. Exp. Biol.*, vol. 202, no. 6, pp. 661–674, Mar. 1999.
[47] K. Wada, M. Saito, and H. Yamaguchi, "Development of the waste mud treatment system for drilling vessel 'CHIKYU,'" in *Proc. IEEE OCEANS*, May 2007, pp. 1–8. doi: 10.1109/OCEANSAP.2006.4393841.
[48] K. Isaka, N. Tadami, A. Fujiwara, T. Watanabe, M. Sugesawa, Y. Yamada, H. Yoshida, and T. Nakamura, "Study on drilling resistance reduction of a seafloor robotic explorer based on the drilling properties of underwater ground," in *Proc. IEEE/SICE Int. Symp. System Integr. (SII)*, Jan. 2019, pp. 718–723. doi: 10.1109/SII.2019.8700347.
[49] C. Zet, C. Fo al u, and D. Petri or, "Pore water pressure sensor for landslide prediction," in *Proc. IEEE SENSORS*, Nov. 2015, pp. 1–4. doi: 10.1109/ICSENS.2015.7370264.
[50] A. M. D. C. Bandara, L. I. N. De Silva, and Y. W. R. Amarasinghe, "Development of an earth pressure cell to evaluate the total and effective stresses of soil," in *Proc. Moratuwa Eng. Res. Conf. (MERCon)*, May/Jun. 2018, pp. 527–532. doi: 10.1109/MERCon.2018.8421980.
[51] K. Terzaghi, "The shearing resistance of saturated soils and the angle between the planes of shear," in *Proc. 1st Int. Conf. Soil Mech.*, vol. 1, 1936, pp. 54–56.
[52] A. W. Skempton, "Terzaghi's discovery of effective stress," in *From Theory to Practice in Soil Mechanics-Selection from the Writings of Karl Terzaghi*. Hoboken, NJ, USA: Wiley, 1996, pp. 42–55.
[53] Z. Szypcio, "Stress-dilatancy of sands with inherent fabric anisotropy for direct shear," in *Proc. IOP Conf., Earth Environ. Sci.*, Jan. 2019, vol. 221, no. 1, Art. no. 012012.
[54] D. W. Taylor, *Fundamentals of Soil Mechanics*. Hoboken, NJ, USA: Wiley, 1948. doi: 10.1097/00010694-194808000-00008.
[55] M. D. Bolton, "The strength and dilatancy of sands," *Géotechnique*, vol. 36, no. 1, pp. 65–78, Mar. 1986.

KEITA ISAKA received the B.S. degree from the Department of Precision Mechanics, Chuo University, Tokyo, Japan, in 2018, where he is currently pursuing the master's degree. His research interest includes the research and development of a seafloor robotic explorer based on earthworm locomotion.

KAZUKI TSUMURA received the B.S. degree from the Department of Precision Mechanics, Chuo University, Tokyo, Japan, in 2019, where he is currently pursuing the master's degree. His research interests include the research and development of a seafloor robotic explorer based on earthworm locomotion.

TOMOKI WATANABE received the B.S. degree from the Department of Precision Mechanics, Chuo University, Tokyo, Japan, in 2019, where he is currently pursuing the master's degree.

His research interests include the research and development of a lunar surface explorer based on earthworm locomotion.

WATARU TOYAMA is currently pursuing the master's degree with Chuo University. His research interests include the research and development of a lunar surface explorer based on earthworm locomotion.

MAKOTO SUGESAWA graduated from the Department of Electronics and Electrical Engineering, Nihon Kogakuin College, Tokyo, Japan, in 1983. From 1983 to 2010, he was an Engineer with an electrical manufacturer. In 2010, he joined the Japan Agency for Marine-Earth Science and Technology. His research interests include the research and development of autonomous underwater vehicles.

YASUYUKI YAMADA (M'12) received the B.S., M.S., and Ph.D. degrees from Keio University, Japan, in 2009, 2011, and 2013, respectively. From 2013 to 2014, he was a Postdoctoral Researcher with the Tokyo Institute of Technology. He was also with Keio University. From 2014 to 2015, he was an Engineer with Nissan Motor Company Ltd. From 2015 to 2018, he was an Assistant Professor with Chuo University. He was also a Visiting Assistant Professor with the Dyson School of Design Engineering, Imperial College London, in 2018. In 2018, he joined Tokyo Denki University, where he is currently an Assistant Professor with the Department of Design Engineering and Technology. He is also an Associate Professor in the research and development initiative with Chuo University. His research interests include the applications of mechanism and soft actuator, design engineering, smart mechanism, and bio-inspired robotics. He is a member of the JSME, JFPS, SICE, and AAAS.

HIROSHI YOSHIDA graduated from the Tokyo Metropolitan College of Technology, Tokyo, Japan, in 1985. He received the Ph.D. degree from the Graduate School of Natural Science and Technology, Kanazawa University, Kanazawa, Japan, in 1999. In 2002, he joined the Japan Agency for Marine-Earth Science and Technology. His research interests include a seafloor robotic explorer and marine robotics.

TARO NAKAMURA (M'04) was born in 1975. He received the B.S., M.E. and M.S., M.E. degrees in mechanical engineering from Akita University, Akita, Japan, in 1997 and 1999, respectively, and the Ph.D. degree from Shinshu University, Nagano, Japan, in 2003. From 1999 to 2003, he was a Research Associate with Akita Prefecture University, Akita. In 2004, he was a Lecturer with the Faculty of Science and Engineering, Chuo University. From 2006 to 2013, he was an Associate Professor with Chuo University, Tokyo, Japan, where he has been a Professor, since 2013. From 2012 to 2013, he was a Visiting Professor with the Swiss Federal Institute of Technology Lausanne, EPFL, Lausanne, Switzerland. He is also the CEO with Solaris, Inc. His research interests include development and control such as an artificial muscle, functional fluid, and development and applications of biorobotics.